Enhancement of Congo red dye removal efficiency using Mg-Fe-layered double hydroxide

Hadja Alia Tabti[1] · Baghdad Medjahed[2] · Mohamed Boudinar[3] ·
Abdelkader Kadeche[1] · Noria Bouchikhi[1] · Amina Ramdani[4,5] · Safia Taleb[4] ·
Mehdi Adjdir[6,7]

Abstract

In this study, Mg-Fe(II)-Al-layered double hydroxide with different molar ratios Fe/Al ($Mg_{0.80}$-$Fe_{0.14}$-$Al_{0.06}$-LDHs and $Mg_{0.80}$-$Fe_{0.20}$-$Al_{0.00}$-LDHs) was prepared via a co-precipitation method at pH constant of 9.5 for a potential application as an efficient Congo red dye removal. The products are characterized by X-ray diffraction, Fourier transform infrared spectroscopy, Brunauer–Emmet–Teller, and X-ray photoelectron spectroscopy. The X-ray diffraction patterns showed that both Mg-Fe-Al-LDHs synthesized with two molar ratios Fe/Al were successfully synthesized without significant impurities. The surface area of Fe-LDHs was about 98 m^2/g. The prepared $Mg_{0.80}$-$Fe_{0.14}$-$Al_{0.06}$-LDHs was utilized for the removal of Congo red (CR) dye. Different parameters such as composite dosage, solution pH, contact time, and initial dye concentration were used to evaluate the adsorption process of CR dye. The results indicated that the optimal dose and contact time were 0.05 g and 5 min, respectively. The CR dye adsorption capacity increased with the increase of initial pH from 5 to 7. The isotherm and kinetics models of adsorption were studied. The adsorption kinetic fits the pseudo-second-order kinetic model with a high degree of correlation coefficient. The adsorption isotherm describes an appropriate fit to the Langmuir model with a maximum adsorption q_m around 11 mg/g. The mechanism interaction study of CR dye molecule on Fe-LDHs was discussed, and it can be attributed to the existence of different forces as hydrogen bonding and electrostatic attraction.

Keywords LDHs · XRD · Adsorption · Congo red · Dyes

✉ Hadja Alia Tabti
  hadjaalia.tabti@gmail.com

Extended author information available on the last page of the article

Introduction

A healthy lifestyle requires the consumption of clean water and a safe environment. Today, water pollution with heavy metals, organic dyes, and industrial discharges has sparked global concern. Dyes are colorful organic compounds that can be used to color textiles, paper, silk and wool, cotton, paint, and in cosmetics field [1–3]. Natural dyes were typically produced from materials such as plants and insects. They have been in use for over 5000 years [4]. However, the disadvantage of natural dyes was their limited variety. So, because of their low cost and wide range of new colors, synthetic dyes have largely replaced natural dyes [5]. In addition, due to their complex structure and their xenobiotic properties, dyes are frequently poorly biodegradable. It has been reported that around 104 dyes are produced each year worldwide [6]. It has been reported by many researchers [7] that every year around 7105 tons of dyes are released, and due to their high solubility in water they are widely dispersed in the environment, causing problems in aquatic life and human health. In this context, several techniques, such as adsorption [8–10], filtration [11], ion exchange [12, 13], biological treatment [13, 14], coagulation [15], and photocatalyst [16, 17], are used to remove toxic colorants from aqueous media. Varieties of adsorbents have been studied in the literature for the removal of these compounds from wastewater. Among these adsorbents clay [18–21], fly ash [22], activated carbon, metal oxide [23], and layered double hydroxide (LDH) [24]. The adsorption capacities of Congo red (CR) [25–27], methyl orange (MO) [28, 29], methylene bleu (MB) [30], and indigo carmine (IC) dyes by calcined and uncalcined LDH were widely studied [31]. The results indicated a good ability of adsorption of dyes onto LDHs. Sriram et al. [32] investigated the CR adsorption by DE-LDHs with a removal efficiency of more than 80%. Shabbir et al. [33] studied adsorption of CR onto Mg-Fe-LDHs for textile dye adsorption, they found Mg-Fe-LDHs suitable for CR adsorption. In the present study, we are concerned with synthesized of Mg-Fe-Al-LDHs with two different molar ratios Fe/Al ($Mg_{0.80}$-$Fe_{0.14}$-$Al_{0.06}$-LDHs and $Mg_{0.80}$-$Fe_{0.20}$-$Al_{0.00}$-LDHs). The obtained materials were characterized by XRD, FTIR, BET, and XPS. Chemical properties of these materials were investigated by XRD, FTIR, and XPS. The $Mg_{0.80}$-$Fe_{0.14}$-$Al_{0.06}$-LDHs was used as an adsorbent for the removal of CR dye from an aqueous solution. Effects of several experimental parameters including contact time, solution pH, dosage composite, and initial dye concentration were investigated to determine the optimum conditions for enhancing CR dye removal. The kinetic models, isotherms, and possible mechanism adsorption of CR dye into Fe-LDHs were also studied.

Experimental

Chemical reagents

Analytical reagents for the preparation of all catalysts including magnesium sulfate monohydrate Mg $(SO_4)0.1H_2O$ 97%, iron chloride tetrahydrate Fe $(Cl_2)0.4H_2O$ 99% were purchased from Sigma-Aldrich. Aluminum nitrate nanohydrate Al $(NO_3)_3.9H_2O$ 98% was obtained from Fluka. Sodium carbonate Na_2CO_3 98%, sodium hydroxide NaOH 99%, and hydrochloric acid HCl 37% were purchased from Sigma-Aldrich. The Congo red dye having molecular formula $C_{32}H_{22}N_2Na_2O_6S_2$, $M_w = 696.98$ g/mol and $\lambda_{max} = 500$ nm was acquired from Sigma-Aldrich. The stocks solution was prepared by dissolving in 1000 mL of deionized water and subsequently diluting to the desired concentrations. All chemical reagents were used without any purification.

Synthesis of Mg-Fe-Al-LDHs

Mg-Fe-Al-LDHs samples were synthesized by simple co-precipitation method reported by Tabti et al. [34] with molar ratios Fe/Al ($Mg_{0.80}$-$Fe_{0.14}$-$Al_{0.06}$-LDHs and $Mg_{0.80}$-$Fe_{0.20}$-$Al_{0.00}$-LDHs). A solution contains $MgSO_4.1H_2O$, $FeCl_2.4H_2O$, and $Al(NO_3)_3 \cdot 9H_2O$ with different molar ratios Fe/Al. Some amounts of $MgSO_4$, $FeCl_2$, and Al $(NO_3)_3$ were mixed together, and then, 1 mol of NaOH and 100 ml of Na_2CO_3 (0.42 M) were slowly added to the mixture. The resulting suspension was stirred for 24 h at 80 °C under reflux. The resulting precipitate was centrifuged and washed with distilled water and dried at 50 °C overnight. Table 1 displays.

Preparation of Congo red solutions

The stock solution of Congo red was prepared by dissolving 1 g/L of CR. This solution was then used to prepare different concentrations (20–100 mg/L). The calibration curve was established by using a UV-Visible spectrophotometer to measuring solutions with different concentrations of CR at $\lambda_{max} = 500$ nm. Congo red elimination studies were performed by varying different parameters such as solution pH, dosage adsorbent, contact time, and the concentration of CR. 15 ml of solution of CR (50 mg/L) was mixed to 50 mg of Fe-LDHs at room temperature. The contact time was also studied in the range of 5 min to 120 min, the adsorbent mass was varied from 10 to 100 mg, the effect of pH was investigated

Table 1 Different molar ratios between Mg^{2+}, Cu^{2+} and Al^{3+}

| Sample | Molar concentration (mol/L) | | | Molar ratios | |
	$|Fe^{2+}|$	$|Mg^{2+}|$	$|Al^{3+}|$	$|Mg^{2+}|/|Al^{3+}|$	$|Mg^{2+}|+|Fe^{2+}|/|Al^{3+}|$
$Mg_{0.80}$-$Fe_{0.14}$-$Al_{0.06}$	0.126	0.72	0.053	13.33	15.67
$Mg_{0.80}$-$Fe_{0.20}$-$Al_{0.00}$	0.180	0.72	0.00	–	–

from 2 to 10, and the pH was adjusted using acid solution (0.1 M HCl) or base solutions (0.1 M NaOH). The adsorption isotherm studies were performed in a concentration ranging from 50 to 100 mg/L. The supernatants were separated by centrifugation (3500 T/min) for 10 min. the concentration of CR was measured by spectrophotometer UV-Visible at $\lambda_{max} = 500$ nm.

The amount of adsorbed CR at equilibrium o the adsorption capacity was determined using Eq. (1)

$$q_e = (c_0 - c_e)\left(\frac{v}{m}\right) \tag{1}$$

where q_e is the adsorption capacity at equilibrium, C_0 and C_e are the concentrations of initial and final CR solutions, V and m are volume of CR solution and mass of adsorbent, respectively. The structure and physicochemical properties of Congo red are given in Fig. 1.

Characterization

XRD patterns were recorded for all the samples in order to check the formation and structure of Fe-LDHs. The diffraction patterns were recorded in the 2θ range of 1–80° with a step size 2θ of 0.02° and a step time of 5 s on a Bruker D5000 diffractometer with CuKα ($\lambda = 0.15406$ nm) radiation equipped with a graphite monochromator and scintillation counter. A CuKα anode was powered with 40 kV and 40 mA. FTIR spectra were recorded in the spectral range of 4000–400 cm^{-1} using a PerkinElmer FTIR spectrophotometer and samples were pressed into KBr disks. The qualitative analysis of the elements comprising the Fe-LDHs samples and the analysis of the electronic binding energy of each element were measured with a X-ray photoelectron spectroscope (ESCALAB 250XI XPS Thermo Company, French, with the light source, the power, and the size of beam spot being AlKα (h$\nu = 1486.6$ eV), 150 W, and 500 m, respectively). Specific surface areas were calculated by using the Brunauer–Emmett–Teller (BET) method.
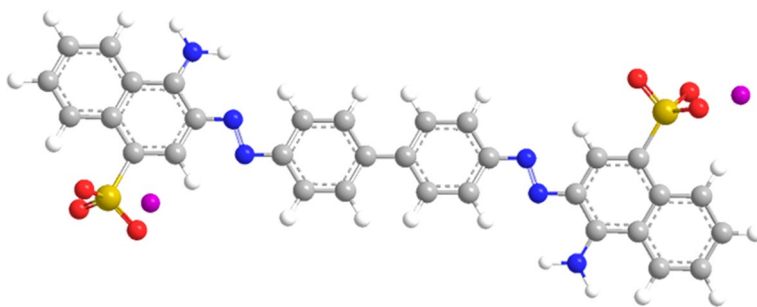

Fig. 1 Structure 3D of Congo red dye

Results and discussion

X-ray diffraction

The X-ray diffraction patterns of Fe-LDHs synthesized with different molar ratios Fe/Al ($Mg_{0.80}$-$Fe_{0.14}$-$Al_{0.06}$-LDHs and $Mg_{0.80}$-$Fe_{0.20}$-$Al_{0.00}$-LDHs) are shown in Fig. 2. Both of Fe-LDHs synthesized with two molar ratios Fe/Al present all the characteristic reflections of hydrotalcite like type. The diffractions peaks are typical of layered double hydroxide structure according to Yi et al. [35], Parida et al. [36]. The diffractograms of $Mg_{0.80}$-$Fe_{0.14}$-$Al_{0.06}$-LDHs and $Mg_{0.80}$-$Fe_{0.20}$-$Al_{0.00}$-LDHs revealed the presence of intense and symmetrical reflections at a low angle of $2\theta = 11.42°$, 23.02° and 31.6° indexing to the plans (003), (006), and (009) which shows a high crystallinity of the synthesis Fe-LDHs [37]. The appearance of broad and asymmetric reflections peaks belongs to the layered double hydroxide structure namely (015) and (018) at $2\theta = 39°$, 46°. The two reflections of (110) and (113) at $2\theta = 60.02°$ and 61.34°, respectively, can be clearly distinguished asserts a good crystallinity under rhombohedral lattice [38]. These major peaks are in agreement with the previous literature [39–42].

It is very important to motion that to synthesize LDHs, it should mix between two cations divalent and trivalent; however, we have successfully synthesized $Mg_{0.80}$-$Fe_{0.20}$-$Al_{0.00}$-LDHs from Mg^{2+} and Fe^{2+}. This can be explained by the oxidation effect of Fe^{2+} to Fe^{3+} during the synthesis due to the basic pH of the solution. Manohara et al. [43] reported that Fe-LDHs synthesized by incorporation of Fe^{3+} are more complex than LDHs containing ions such as Al^{3+}, this is maybe ascribed to the difference in the solubility between $Fe(OH)_3$, $Mg(OH)_2$,
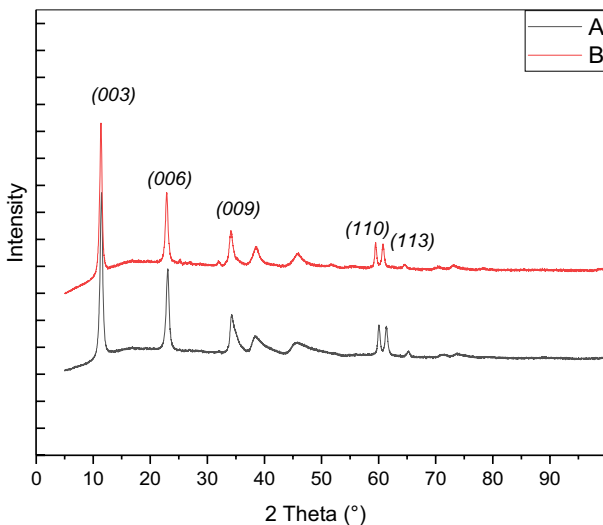
Fig. 2 XRD patterns of Mg-Fe-Al-LDHs synthesized with different Fe/Al molar ratios ($a = Fe_{0.14}$-$Al_{0.06}$, $b = Fe_{0.20}$-$Al_{0.00}$)

Table 2 Experimental parameters of the prepared LDHs samples

| Samples	$2\theta_{(003)}$	$d_{(003)}$	a (Å)	c (Å)	$\beta_{(003)}$	$D^{¤}_{(003)}$	$D^{¤}_{(110)}$
Fe$_{0.14}$-Al$_{0.06}$	11.349	7.789	3.091	23.369	0.539	14.794	18.299
Fe$_{0.20}$-Al$_{0.00}$	11.359	7.783	3.104	23.350	0.525	15.188	18.473

d basal spacing, *a*, *c* Lattice cell parameters: ($c = 3d_{003}$, $a = 2d_{110}$). $D^{¤}$ particle sizes calculated using the Scherrer equation. *β* full width at half maximum

and Al(OH)$_3$ [44]. It is also observed that no iron oxide phase has been detected, indicating that all the amount of iron has reacted [45].

Table 2 presents the experimental parameter, where 'a' is the distance metal–metal in the framework, it was calculated from the plan (110) ($a = 2d_{110}$), whereas the parameter '*c*' corresponds to three times the layer-to-layer distance ($c = 3d_{003}$) [46]. The basal spacing '*d*' was calculated using Brag's law equation, and '*D*' is the size particles, it was determinate by the Scherrer equation and '*β*' is the full width at half maximum.

According to Table 2, '*a*' parameter values are varied between 3.091 and 3.104 Å this variation is due to the isomorphous substitution and the difference between the ionic radius of Al^{3+} (0.675 Å) and Fe^{3+} (0.785 Å). The interlayer spacing '*d*' corresponding to the plan (003) was equal to 7.78 Å which is in agreement with Lu et al.[47]. The position of the reflection plan (003) has been used to calculate the lattice parameter '*c*' which is around 23.36 Å. This result is similar to those found in previous reports [48, 49]. For the FWHM, we noticed the decrease of '*β*' with the increase of Fe^{2+} content and consequently the increase of the crystallinity. Scherrers' formula was applied to calculate the particle size, its values were varied between 14.79 nm and 15.18 nm for the samples (Mg$_{0.80}$-Fe$_{0.14}$-Al$_{0.06}$-LDHs and Mg$_{0.80}$-Fe$_{0.20}$-Al$_{0.00}$-LDHs), respectively, this result is similar to that found by Abdel Moaty et al. [40]. The particle size played an important role in the catalytic activity of materials.
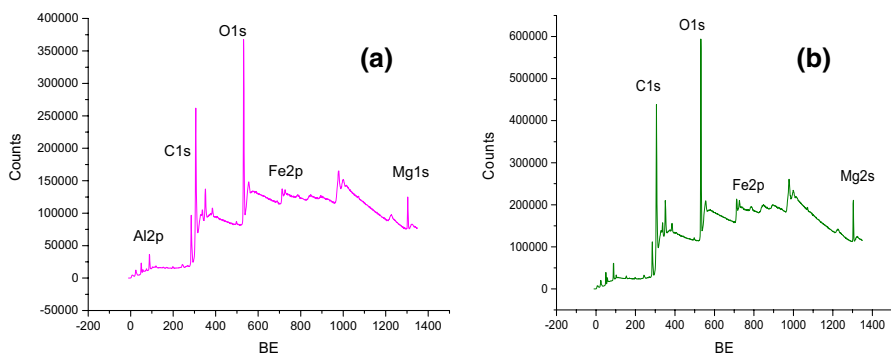
Fig. 3 XPSspectra of Mg-Fe-Al-LDHs synthesized with different Fe/Al molar ratios (**a** = Fe$_{0.14}$-Al$_{0.06}$, **b** = Fe$_{0.20}$-Al$_{0.00}$)
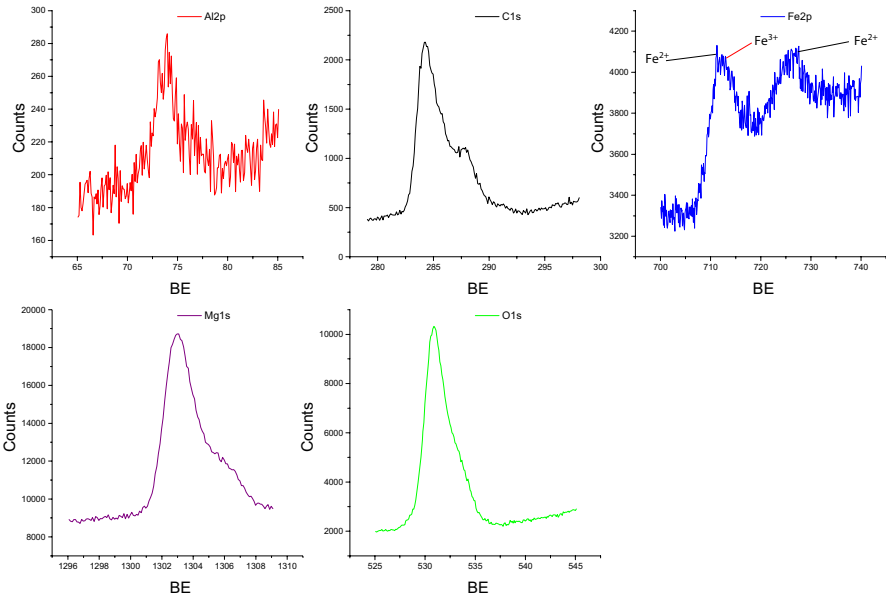
Fig. 4 XPS spectra patterns of Fe-LDHs synthesized with molar ratio Fe/Al ($Fe_{0.14}$-$Al_{0.06}$)
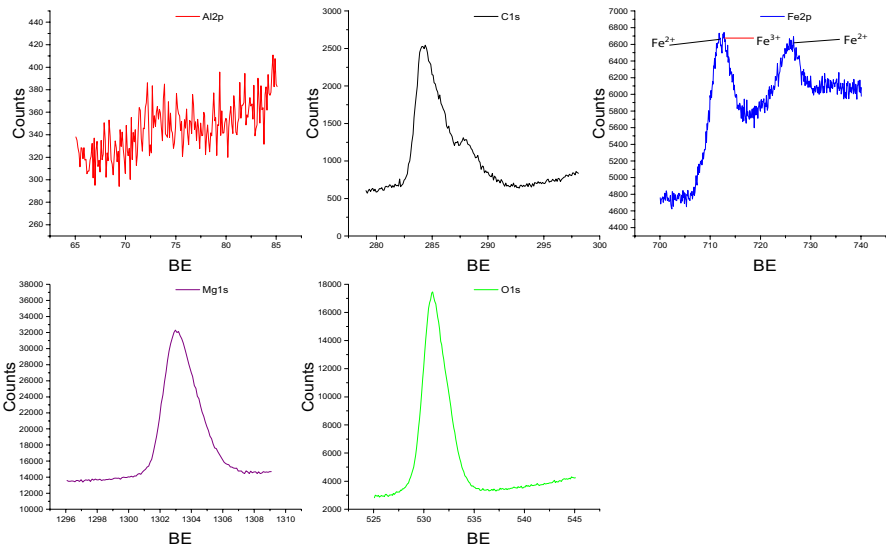

Fig. 5 XPS spectra patterns of Fe-LDHs synthesized with molar ratio Fe/Al ($Fe_{0.20}$-$Al_{0.00}$)

XPS analysis

XPS spectra of Fe-LDHs synthesized with different molar ratios Fe/Al are shown in Fig. 3. The XPS survey was used to identify the surface properties of our materials

and to determine the configuration electronic of metal coexisting in the samples. The XPS spectra revealed the existence of C, O, Al, Mg, and Fe atoms on the surface of Fe-LDHs.

Figures 4 and 5 present the XPS spectra of Fe-LDHs, respectively, for the nanocomposite $Mg_{0.80}$-$Fe_{0.14}$-$Al_{0.06}$-LDHs and $Mg_{0.80}$-$Fe_{0.20}$-$Al_{0.00}$-LDHs. The peak of C1s is observed at the BE values of 284.9 eV corresponding to the contamination carbon. Another peak of C1s is observed at 288 eV that indicates the presence of carbonate anion in the interlamellar space of Fe-LDHs.

For O1s peak which is presented in Fig. 4 and 5, we noticed the appearance of a peak located at 532.5 eV which is characterized by high intensity, it is attributed to the oxygen of carbonate (C=O). The peak of Mg1s is founded at bending energy value 1304 eV indicating that Mg^{2+} is present as MgO [50, 51].

For the synthesis samples, as shown in Figs. 4 and 5, the binding energy of the peak Al2p was 74 eV, which points out the presence of octahedral Al^{3+} in the brucite layer of LDHs synthesized with the molar ratio Fe/Al ($Fe_{0.14}$-$Al_{0.06}$), whereas this peak disappeared in the sample $Mg_{0.80}$-$Fe_{0.20}$-$Al_{0.00}$-LDHs.

For iron, as shown in Figs. 4 and 5, we observed the appearance of two peaks Fe2$p_{3/2}$ and Fe2$p_{1/2}$ at the regions of 710 eV and 725 eV, respectively, for Fe^{2+} corresponding to FeO. Also, we observed the existence of peak Fe2$p_{3/2}$ at bending energy 712 eV corresponding to Fe^{3+}. This result confirms the oxidation of Fe^{2+} to Fe^{3+} takes place during the synthesis and confirmed by X-ray diffraction for the sample $Mg_{0.80}$-$Fe_{0.20}$-$Al_{0.00}$-LDHs. Based on this result, the synthesis of a high ordered LDHs can be realized without a trivalent cation, the diffractogram pattern of this sample proves the formation of a high-ordered hydrotalcite phases [33, 52–54].

Fourier Transform Infrared (FTIR) spectroscopy

Figure 6 shows the FTIR spectra of Fe-LDHs before and after CR adsorption. The FTIR spectrum of Fe-LDHs exhibited a broad and intense absorption peak at 3600 cm^{-1} region, which is related to the isolated Al–OH group. The broad band centered at 3462 cm^{-1} is attributed to the -OH stretching vibration mode due to the presence of hydroxyls groups in the LDHs and the interlayer water [36, 55, 56]. The hydrogen band that connects both interlayer water and carbonate ions in the interlayer space was responsible for the small band at approximately 3076 cm^{-1}, this mode was directly related to the H_2O–CO_3^{-2} mode of bridge formation. The band at 1623 cm^{-1} is due to the –OH bending vibration of water molecules in the interlayer space (deformation mode of H–O–H) as reported by Ferreira et al. [58], Yi et al. [35], and Extremera et al. [57]. The band at 1347 cm^{-1} is due to the stretching vibration of carbonate groups which is converted from CO_2 captured from the air during the synthesis of Fe-LDHs and it is becoming weaker after CR adsorption which is attributed to the mode of υ_3 asymmetric stretching of CR dye anions [59, 60]. The bands in the range of 400 cm^{-1} and 1000 cm^{-1} are attributed to the M–O or O–M–O vibrational mode and the stretching mode of M–O–M bands (M=Mg, Fe and, Al). An additional peak was appeared after CR adsorption at 1020 cm^{-1} due to

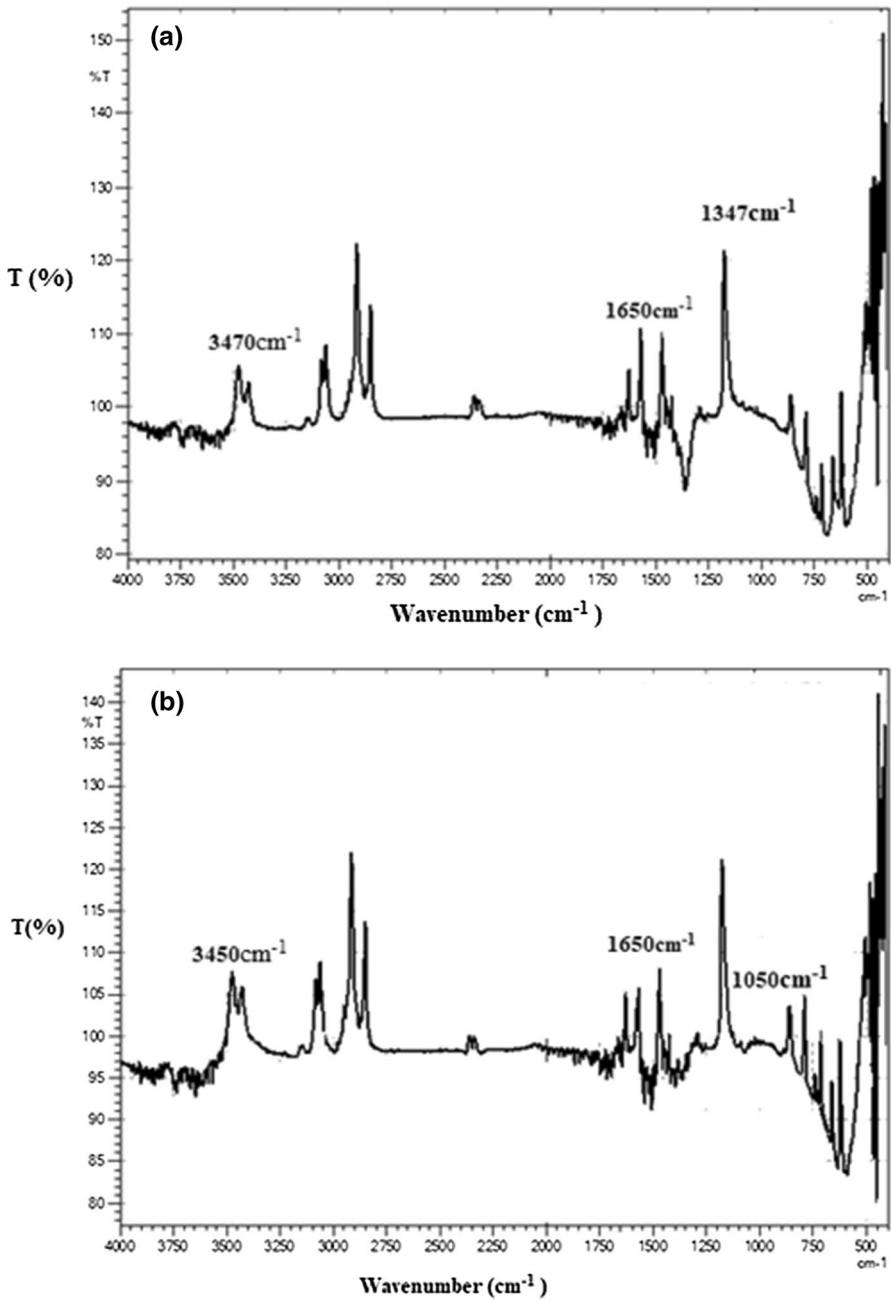**Fig. 6** The FTIR spectrum of $Mg_{0.80}$-$Fe_{0.14}$-$Al_{0.06}$-LDHs (**a**) and $Mg_{0.80}$-$Fe_{0.14}$-$Al_{0.06}$-LDHs-CR (**b**)

the symmetric stretching of the sulfonate group ($-SO_3^-$) present in CR dye [61]. It is completely consistent with the description in the literature [39, 62, 63].

N₂-adsorption–desorption

N_2-adsorption–desorption isotherm for Fe-LDHs synthesized is revealed in Fig. 7. According to the classification of materials in IUPAC, the isotherm exhibited type II revealing the presence of microporous or non-porous materials with a hysteresis loop that occurs during desorption. The position of "β" inflections points in the low relative pressure range P/P_0 indicating a low affinity between adsorbent (LDHs) and adsorbate (N_2). The value of the specific surface area was calculated, it is around 98m²/g.

Zero-point charge of Fe-LDHs

Determination of surface charge of adsorbent is important to know the removal capacity of dye by this adsorbent from aqueous solutions. We can calculate this surface charge by zeta potential using the method of Sontheimer [64]. The zeta potential was calculated between pH 2 and 12 for Fe-LDHs as shown in Fig. 8. Zero-point charge (pH_{pzc}) of Mg-Fe-Al-LDHs is around 9.2, the Fe-LDHs has a positive surface charge below pH9.2 and CR dye molecule can be easily adsorbed from pH 2 and pH 9.2; however, the surface of Fe-LDHs is negatively charged above pH_{pzc} value; therefore, the adsorption capacity of CR dye is unfavorable in this range of pH ($pH \geq pH_{pzc}$) [65–67].
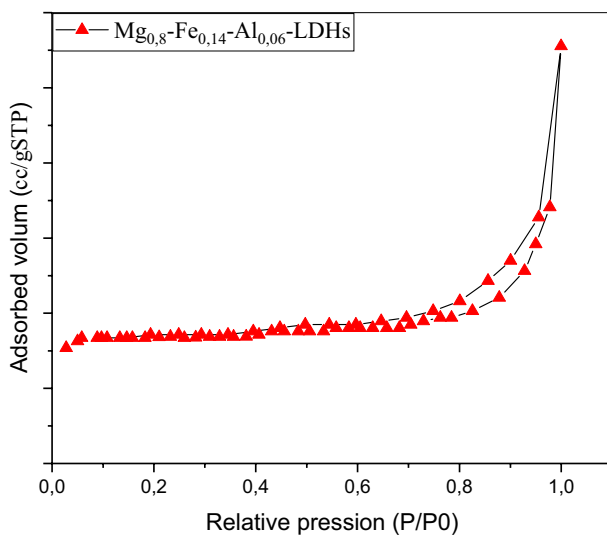
Fig. 7 Adsorption–desorption isotherm of $Mg_{0.80}$-$Fe_{0.14}$-$Al_{0.06}$-LDHs
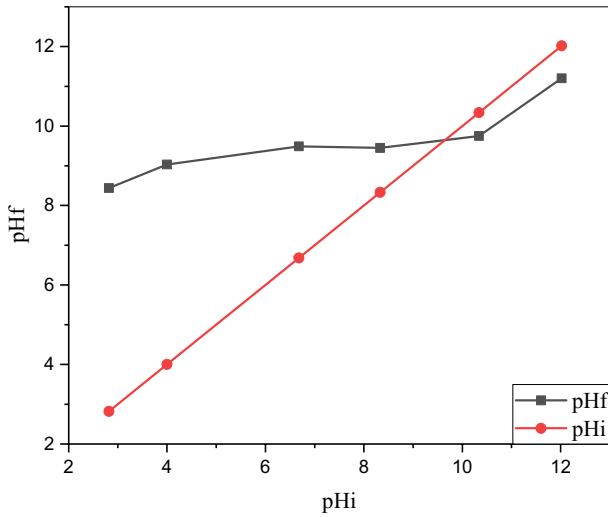
Fig. 8 Zero-point charge of $Mg_{0.80}$-$Fe_{0.14}$-$Al_{0.06}$-LDHs

Adsorption of CR dye by Fe-LDHs

Effect of contact time

The effect of contact time on the adsorption of CR dye by Fe-LDHs was investigated. The experiments have been performed at different contact time from 5 to 120 min with 50 mg/L of CR dye and 50 mg of Fe-LDHs at room temperature. From the results shown in Fig. 9, it is very clear that the adsorption rate is very fast and

Fig. 9 Effect of contact time on CR dye capacity adsorption using Fe-LDHs (pHi = 8.7, m = 50 mg, Ci = 50 mg//L and 298 K)

showed that the elimination of CR by Fe-LDHs reached equilibrium at 5 min. This can be attributed to the contribution of large number of vacant active sites on the LDH. By increasing adsorption time, the removal capacity of CR dye becomes constant because the residual vacant active sites o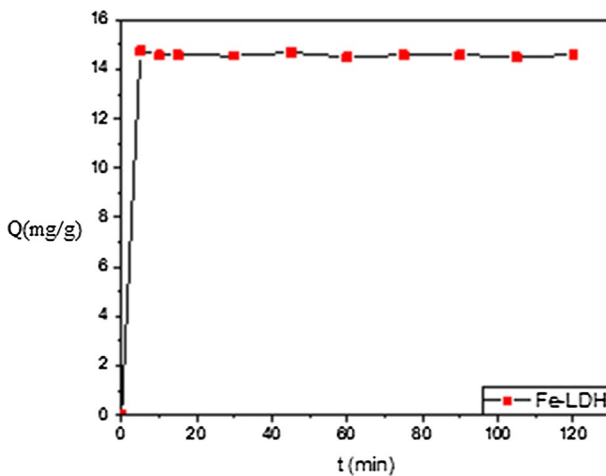f Fe-LDHs attended the saturation and therefore, the adsorption capacity q_{max} was about 14.74 mg/g. These results are in agreement with those found by Lafi et al. [25], Sriram et al. [32], Shabbir et al. [33] who founded that the equilibrium time of adsorption of CR is about 20 and 30 min.

Effect of adsorbent mass

The effect of adsorbent mass on the immobilization of CR dye by Fe-LDHs is given in Fig. 10. It was tested by adding adsorbent mass in the range 10 to 100 mg in the aqueous solution of CR with an initial concentration of 50 mg//L, contact time 5 min at temperature room. From the result of Fig. 10, the CR dye removal capacity by Fe-LDHs increases with increasing the adsorbent mass from 10 mg until the optimum mass 50 mg. However, after 50 mg of adsorbent amount, there was no discernible difference in removal dye capacity, implying that it had reached saturation since no dye molecules were able to be adsorbed at higher dosages [68], and due to the availability of active sites of adsorbent. Furthermore, the removal capacity has also been influenced by the surface area and surface properties of adsorbents, both of which play major roles in dye removal.

Effect of initial solution pH

Figure 11 presents the effect of pH initial on the adsorption of CR dye by Fe-LDHs. The pH of the solution is important in controlling the adsorption capacity
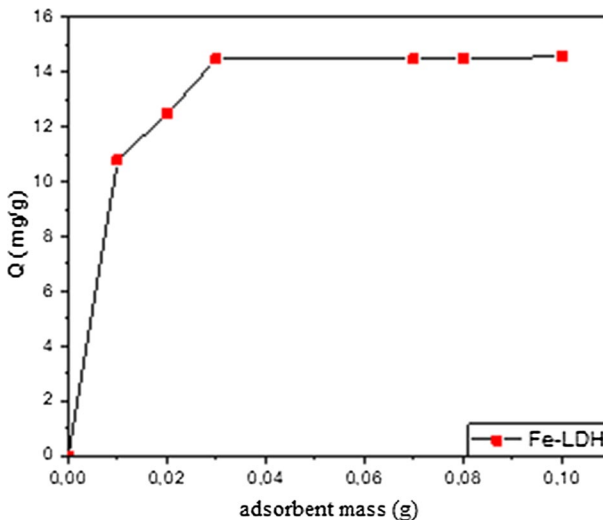
Fig. 10 Effect of adsorbent mass on CR dye capacity adsorption, (pHi = 8.7, t = 5 min, Ci = 50 mg/L and 298 K)
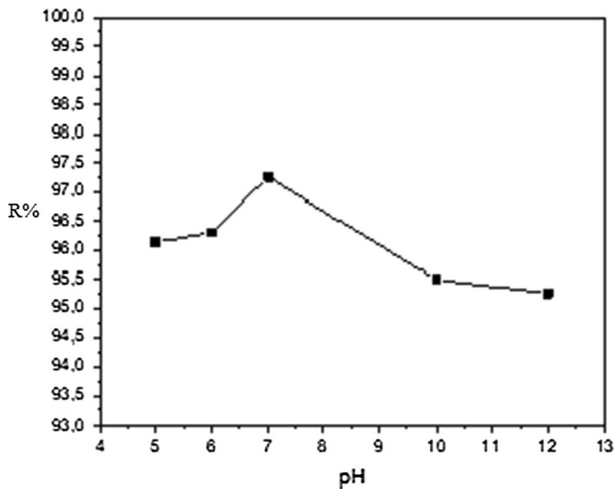
Fig. 11 Effect of initial solution pH on CR dye removal percentage, ($m = 50$ mg, $t = 5$ min, Ci $= 50$ mg/L and 298 K)

of the adsorbent which can be attributed to several parameters at different pH values such as surface charge area of adsorbent and actives sites, so the dye uptake can be related to the actives sites as well as the dye chemistry in solution. During the adsorption processes, various types of interaction have been observed between adsorbent–adsorbate, dye–dye, hydrogen bond, and hydrophobic interaction [69]. It is important to know that CR dye is not stable below pH $= 5$, in the latest study, the pH was varied from 5 to 10 to remove CR dye using 50 mg of adsorbent. As can be seen from Fig. 11, CR dye adsorption rate increases gradually from pH $= 5$ to pH $= 8$ and then decreases continuously after pH $= 8$. This finding can be explained by the electrostatic interaction between the CR dye molecules and Fe-LDHs. In an acid medium, the H^+ ions are very mobile, which will neutralize the negative charge of the sulfonate dye groups. At low pH and before the (PZC), the surface of the adsorbent becomes positively charged which increases the adsorption capacity of CR negatively charged via electrostatic forces of attraction between sulfonate groups and layered positively charged, also the formation of hydrogen bonds between hydroxyl groups of Fe-LDHs and atoms of N of CR dye [70]. In the basic medium and when the pH values exceed (PZC), the surface becomes negatively charged which creates an attraction between hydrogen groups and CR dye molecule; however, there are ions competition between OH ions and CR dye species leading to lower removal efficiency. Fe-LDHs had the highest dye removal efficiency (97%) at pH $= 7$. After pH $= 9$, the dye removal rate decreases because the surface of Fe-LDHs becomes negatively charged which repels the negatively charged dye. Similar results have been reported by Sriram et al. [32].
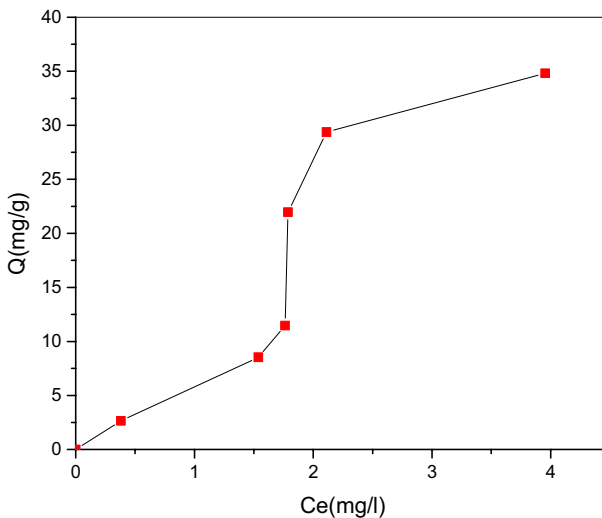
Effect of initial adsorbate concentration

The influence of the concentration of CR dye on removal capacity was carried out. It was tested by adding 50 mg of Fe-LDHs in the aqueous solution of CR with different concentrations (10–120 mg/L), contact time 5 min, pHi 8.7, and temperature room. The results are shown in Fig. 12, which reveals that Fe-LDHs removed a significant amount of CR dye from the aqueous solutions. The adsorption efficiency increases with the increase of the concentration of CR dye until a certain concentration, which could be attributed to the fact that the adsorbents had a limited number of actives sites that have become saturated after a certain concentration. This also suggests that the adsorption process begins with monolayer adsorption in low concentrations of CR dye, progresses to multilayer adsorption as the concentration increases which reaches saturation at high initial concentrations [33].

Adsorption kinetic

Adsorption mechanisms frequently involved chemical reactions between adsorbate and functional groups on the adsorbent surfaces. Several kinetic models have been used to describe the order of adsorbate and adsorbent interactions. In this study, the adsorption controlling mechanism was investigated using pseudo-first-order and pseudo-second-order models (Eqs. 2 and 3). The results are tabulated in Table 3.

$$\log\left(q_e - q_t\right) = \log q_e - \log q_e \left(\frac{k_1}{2.303}\right) \cdot t \tag{2}$$

Fig. 12 Effect of initial CR concentration on CR dye adsorption capacity, ($m = 50$ mg, $t = 5$ min, pHi $= 8.7$ and 298 K)

Table 3 Parameters in the two kinetic models for CR adsorption by Fe- LDHs

| Adsorbent	Pseudo-first-order kinetic model				Pseudo-second-order kinetic model		
Fe-LDHs	$q_{e,exp}$	K_1	$q_{e,cal}$	R^2	K_2	$q_{e,cal}$	R^2
	14.74	0.0639	1.6053	0.4934	0.21160	14.72	0.999

$q_{e,exp}$ (mg/g), $q_{e,cal}$ (mg/g), k_1 (min^{-1}), k_2 (g/mg min)

$$\frac{t}{q_t} = \frac{1}{\left(k_2 q_e^2\right)} + \frac{1}{q_e}t \tag{3}$$

According to the results, the pseudo-second-order model fits the data better than the pseudo-second-order model. The correlation coefficient for the pseudo-second-order model (R^2) was higher than for the pseudo-first-order model, its value is equal to 0.99 which is closer to 1. Furthermore, when compared to the pseudo-first-order kinetic model, the value of q_e, which is referred to as the calculated adsorption quantity at equilibrium, matches perfectly with the experimental value $q_{exp} = 14.74$ mg/g. As a result of these considerations, the adsorption kinetics of CR dye by Fe-LDHs obeys the pseudo-second-order model. This result is similar to that found by Lafi et al. [25], Chilukoti et al. [71].

Adsorption isotherms

Figures 13 and 14 show the adsorption isotherm of Langmuir and Freundlich linear fitting models. The adsorption isotherms were used to evaluate the adsorption capacity

Y=6,52338X+0,10561
R^2=0,964
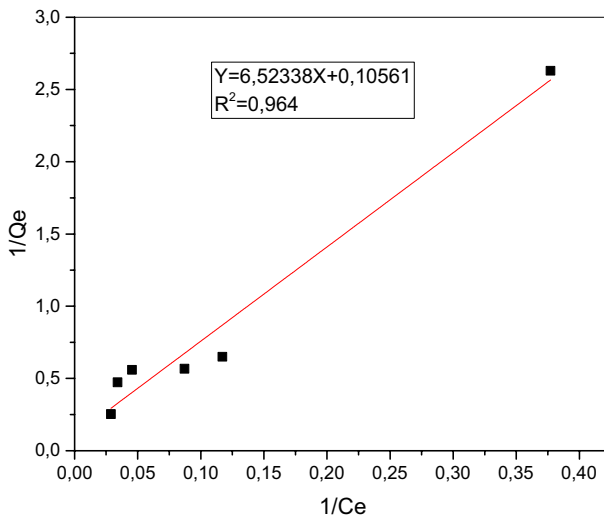
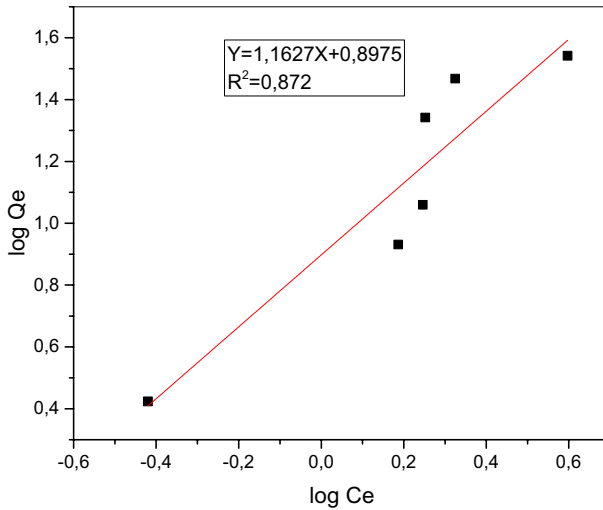**Fig. 13** Linear plot of Langmuir model isotherm

Fig. 14 Linear plot of Freundlich model isotherm

of Fe-LDHs at various equilibrium adsorbate concentrations which provide us with information about the adsorbent's maximum adsorption capacity q_m, adsorbent surface properties, also the nature of CR adsorption onto the adsorbent surface. The Langmuir and Freundlich isotherm models were used to analyze the adsorption experimental data, they can be expressed, respectively, by Eqs. 4 and 5:

$$\frac{Ce}{q_e} = \frac{Ce}{(q_m \cdot k_L)} + \frac{1}{q_m} \tag{4}$$

$$\log q_e = \log k_F + \frac{1}{n} \log C_e \tag{5}$$

where (q_e) and (q_m) are the adsorption capacities on equilibrium and maximum adsorption capacities (mg/g), (Ce) is the concentration of dye (mg/L), K_L and K_F are constants of Langmuir and Freundlich models, respectively. The parameters of isotherms models were given in Table 4.

The Fe-LDHs isotherms and Table 4 showed that the correlation coefficient (R^2) of the Langmuir model was well fitted when compared to the Freundlich model and its maximum adsorption capacity (q_m) was found to be 10 mg/g. High K_L values represent an admirable adsorption process, and these values revealed a higher affinity between the CR molecule dye and Fe-LDHs surfaces. These findings are in agreement with

Table 4 Parameters of the Langmuir, Freundlich isotherm models for CR dye adsorption onto Fe-LDHs

Adsorbent	Freundlich model			Langmuir model		
	K_f	n	R^2	K_L	q_m	R^2
Fe-HDLs	1.766	0.860	0.872	7.899	9.4689	0.964

Shabbir et al. [33] who reported that the surface of Fe-LDHs is homogeneous and that the adsorption mechanism of monolayer uptake.

Mechanism of CR adsorption on Fe-LDHs

In general, the mechanism of adsorption of CR dye on the surface of LDHs includes several interactions as shown in Fig. 15. The first is the formation of two hydrogen bonding namely the hydrogen dipole–dipole between H-donor of hydroxyl groups of Fe-LDHs and H-acceptor of the nitrogen atom of dye, and Yoshida H bonds which is hydrogen bonding between hydroxyl groups at the adsorbent surface and the aromatic ring of dye, n–π interaction between aromatic rings of dye and carbonyl oxygen groups present on the LDHs surface, then electrostatic interaction between the positively charged LDHs sheet and sulfonate groups ($-SO_3^-$) of CR dye molecules. These results are in agreement with Sriram et al. [32], Shabbir et al. [33] who reported that FTIR spectra of LDHs after CR adsorption revealed the appearance of the bond at 1020 cm^{-1} which was caused by symmetric stretching of sulfonate groups [61], the intensity of characteristic bond of carbonate anions decreased which indicated interlayer exchange between carbonate anions and CR molecules [72]. These findings are qualitatively in good agreement with the results of the FTIR spectrum of our materials.

Comparison with other adsorbents

Different adsorbents were used to remove Congo red from the aqueous solution, Table 5 shows the maximum CR removal efficiency with some materials from the literature. When compared to previously reported adsorbents, the current study's
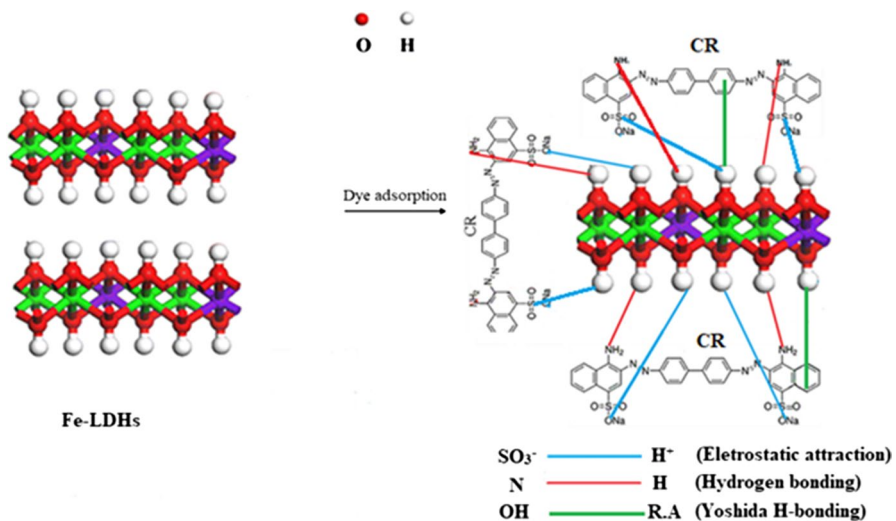

Fig. 15 Schematic representation of CR adsorption mechanism onto Fe-LDHs various molar ratios of Mg^{2+}, Fe^{2+}, and Al^{3+}

Table 5 Comparison of adsorption capacities adsorbents toward CR dye

Adsorbent	Contact time (min)	$C_{initial}$ (mg/L)	Q_{max}(mg/g)	References
Cu-Mg-LDHs	60	20	50	[73]
Ni-Fe-LDHs	50	25	8.79	[74]
Mg-Fe-LDHs	50	25	7.61	[74]
Bentonite	90	50	13.47	[75]
BTMA-Ben	90	50	15.34	[75]
HDTM-Ben	90	50	16	[75]
THMA-Ben	90	50	15.3	[75]
Prepared activate carbon from coffee	240	20	9.41	[76]
B–Mg/Al–LDH	–	–	166	[77]
NH$_2$–Mg/Al–LDH–EDTA	–		632	[78]
IL–Mg/Al–LDH	120		288	[79]
Zn–Fe$_2$O$_4$–Mg/Al–LDHs			294.14	[80]
Ni/Al–CO$_3$–LDH	100		168	[81]
Mg/Al–LDH–CF	10		271	[82]
Mg-Fe-Al-LDHs	5	50	14.75	This study

Fe-LDHs adsorbent showed a high adsorption capacity for the adsorption of CR from an aqueous solution. This finding has suggested the possibilities for practical applications of Fe-LDHs on an industrial scale as real alternative adsorbents.

Conclusion

In this work, Fe-LDHs were successfully synthesized using a simple co-precipitation method with molar ratios Fe/Al ($Mg_{0.80}$-$Fe_{0.14}$-$Al_{0.06}$-LDHs and $Mg_{0.80}$-$Fe_{0.20}$-$Al_{0.00}$-LDHs). The prepared Fe-LDHs have formed a crystalline layered structure as shown by XRD. XPS analysis revealed the presence of Mg, Fe, O, and C on the surface of Fe-LDHs, the spectrum corresponding to Al2p appeared at 72 eV only for the products synthesized with the molar ratio Fe/Al ($Mg_{0.80}$-$Fe_{0.14}$-$Al_{0.06}$-LDHs).

The synthesis of high ordered LDH can also be realized only by divalent cation. Congo red dye was removed by Fe-LDHs from a solution at an initial concentration of 50 mg/L. The adsorption kinetics results showed that the adsorption process reached equilibrium in about 5 min which is faster than other adsorbents. The CR removal was increased by increasing the initial concentration of CR dye in the solution. pH had a significant effect on CR dye adsorption by Fe-LDHs. The CR dye's maximum adsorption rate was achieved at pH = 7. The equilibrium isotherm was described well by the Langmuir model and the adsorption kinetics data fit pseudo-second-order model with a correlation coefficient of 0.99. The adsorption mechanism was explained by the hydrogen bonding and electrostatic forces between CR

dye molecules and Fe-LDHs. According to the results of the current study, Fe-LDHs can be used as an excellent adsorbent of dyes as well as for wastewater treatment.

References

1. M.A.M. Salleh, D.K. Mahmoud, W.A.W.A. Karim, A. Idris, Desal **280**, 1 (2011)
2. M.T. Yagub, T.K. Sen, S. Afroze, H.M. Ang, Adv. Coll. Interface Sci. **209**, 172 (2014)
3. G. Zeng, Z. Ye, Y. He, X. Yang, J. Ma, H. Shi, Z. Feng, Chem. Eng. J. **323**, 572 (2017)
4. R. Kant (2011)
5. H. Gabriel, J. Hong, Res. J. Appl. Sci. **3**, 216 (2008)
6. E. Forgacs, T. Cserhati, G. Oros, Environ. Inter. **30**, 953 (2004)
7. A. Espantaleon, J. Nieto, M. Fernandez, A. Marsal, Appl. Clay Sci. **24**, 105 (2003)
8. L. Ai, C. Zhang, L. Meng, J. Chem, Eng Data **56**, 4217 (2011)
9. S. Dong, J. Feng, M. Fan, Y. Pi, L. Hu, X. Han, M. Liu, J. Sun, RSC Adv. **5**, 14610 (2015)
10. R. Cherrak, M. Hadjel, N. Benderdouche, M. Adjdir, A. Mokhtar, K. Khaldi, A. Sghier, P.G. Weidler, Silic **12**, 927 (2020)
11. Y. Zheng, G. Yao, Q. Cheng, S. Yu, M. Liu, C. Gao, Desal **328**, 42 (2013)
12. J. Labanda, J. Sabaté, J. Llorens, Chem. Eng. J. **166**, 536 (2011)
13. N. Bouchikhi, M. Adjdir, K.C. Bendeddouche, D. Bouazza, A. Mokhtar, F. Bennabi, H.A. Tabti, A. Sehmi, H. Miloudi, Mater. Res. Expr. **6**, 1250 (2020)
14. M. Kornaros, G. Lyberatos, J. Hazar. Mater. **136**, 95 (2006)
15. J. Zhang, S. Chen, Y. Zhang, X. Quan, H. Zhao, Y. Zhang, J. Hazar. Mater. **274**, 198 (2014)
16. A. Elhalil, R. Elmoubarki, M. Farnane, A. Machrouhi, F. Mahjoubi, M. Sadiq, S. Qourzal, M. Abden-nouri, N. Barka, J. Sci, Adv. Mater. Dev. **4**, 34 (2019)
17. A. Elhalil, R. Elmoubarki, M. Farnane, A. Machrouhi, M. Sadiq, F. Mahjoubi, S. Qourzal, N. Barka, Environ. Nano. Monit. Manag. **10**, 63 (2018)
18. M. Toor, B. Jin, Chem. Eng. J. **187**, 79 (2012)
19. A. Kadeche, A. Ramdani, M. Adjdir, A. Guendouzi, S. Taleb, M. Kaid, A. Deratani, Res. Chem. Intermed. **46**, 4985 (2020)
20. M. Boudinar, M. Adjdir, A. Bendraoua, M. Hadjel, C.K. Bendeddouche, R. Chellali, H. Benhaoua, H. Marita, P. Weidler, Environ. Nano Monit. Manag. **8**, 268 (2017)
21. B. Guezzen, M. Adjdir, B. Medjahed, M.A. Didi, P.G. Weidler, Can. J. Chem. **98**, 215 (2020)
22. S. Dong, J. Feng, Y. Li, L. Hu, M. Liu, Y. Wang, Y. Pi, J. Sun, J. Sun, Appl. Catal. B Environ. **152**, 413 (2014)
23. P. Xu, G. Zeng, Sci. Total. Environ. **424**, 1 (2012)
24. A. Zaghloul, R. Benhiti, A.A. Ichou, G. Carja, A. Soudani, M. Zerbet, F. Sinan, M. Chiban, Mater. Today Proc. **37**, 3793 (2021)
25. R. Lafi, K. Charradi, M.A. Djebbi, A.B.H. Amara, A. Hafiane, Adv. Powder Technol. **27**, 232 (2016)
26. R. Wang, Q. Li, N. Duan, T. Zhang, H. Lu, Res. Chem. Intermed. **41**, 7899 (2015)
27. H.-Y. Zhu, R. Jiang, J. Yao, F.-Q. Fu, J.-B. Li, Res. Chem. Intermed. **42**, 4359 (2016)
28. G. Darmograi, B. Prelot, G. Layrac, D. Tichit, G. Martin-Gassin, F. Salles, J. Zajac, J. Phys. Chem. C **119**, 23388 (2015)
29. C. Peng, J. Dai, J. Yu, J. Yin, Aip Adv. **5**, 057138 (2015)
30. M. Zhang, Q. Yao, C. Lu, Z. Li, W. Wang, ACS Appl. Mater. Interface **6**, 20225 (2014)
31. L. El Gaini, M. Lakraimi, E. Sebbar, A. Meghea, M. Bakasse, J. Hazar. Mater. **161**, 627 (2009)
32. G. Sriram, U. Uthappa, D. Losic, M. Kigga, H.-Y. Jung, M.D. Kurkuri, Appl. Sci. **10**, 2285 (2020)
33. R. Shabbir, A. Gu, J. Chen, M.M. Khan, P. Wang, Y. Jiao, Z. Zhang, Y. Liu, Y. Yang (2020) Int. J. Envi-ron. Anal. Chem. **102**
34. H.A. Tabti, M. Adjdir, A. Ammam, B. Mdjahed, B. Guezzen, A. Ramdani, C.K. Benddedouche, N. Bouchikhi, N. Chami, Res. Chem. Intermed. **46**, 5377 (2020)
35. H. Yi, S. Zhao, X. Tang, P. Ning, H. Wang, D. He, Catal. Commun. **12**, 1492 (2011)
36. K. Parida, L. Mohapatra, Chem. Eng. J. **179**, 131 (2012)
37. R. Chitrakar, A. Sonoda, Y. Makita, T. Hirotsu, Sep. Purif. Technol. **80**, 652 (2011)
38. G. Carja, R. Nakamura, H. Niiyama, Appl. Catal. A Gen. **236**, 91 (2002)
39. Y. Guo, Z. Zhu, Y. Qiu, J. Zhao, J. Environ. Sci. **25**, 944 (2013)
40. S.A. Moaty, R.K. Mahmoud, N.A. Mohamed, Y. Gaber, A.A. Farghali, M.S.A. Wahed, H.A. Younes, Water Environ. J. **34**, 290 (2020)

41. K. Yang, Y. Du, J. Shen, X. Lü, Z. Li, Z. Chen, Y. Feng, M. Du, C. Zhu, J. Wuhan Univ. Technol.-Mater. Sci. Ed. **34**, 866 (2019)
42. H. Abdolmohammad-Zadeh, A. Jouyban, R. Amini, Talanta **116**, 604 (2013)
43. G. Manohara, S. Prasanna, P.V. Kamath, Eur. J. Inorg. Chem. **2011**, 2624 (2011)
44. D. Dobos, D. Dobos, *Electrochemical Data: A Handbook for Electrochemists in Industry and Universities* (Elsevier Science and Technology, Amsterdam, 1975)
45. K. Xing, H. Wang, L. Guo, W. Song, Z. Zhao, Coll. Surf. A Phys. Eng. Asp. **328**, 15 (2008)
46. R.R. Delgado, C.P. De Pauli, C.B. Carrasco, M.J. Avena, Appl. Clay Sci. **40**, 27 (2008)
47. Y. Lu, B. Jiang, L. Fang, F. Ling, J. Gao, F. Wu, X. Zhang, Chemosphere **152**, 415 (2016)
48. T. Kameda, J. Oba, T. Yoshioka, J. Environ. Manag. **188**, 58 (2017)
49. C. Lei, X. Zhu, B. Zhu, C. Jiang, Y. Le, J. Yu, J. Hazar. Mater. **321**, 801 (2017)
50. S. Alla, A. Verma, V. Kumar, R. Mandal, I. Sinha, N. Prasad, RSC Adv. **6**, 61927 (2016)
51. F. Khairallah, A. Glisenti, M.M. Natile, A. Galenda, Surf. Sci. Spectra **19**, 23 (2012)
52. K. Parida, M. Satpathy, L. Mohapatra, J. Mater. Chem. **22**, 7350 (2012)
53. F. Ning, M. Shao, S. Xu, Y. Fu, R. Zhang, M. Wei, D.G. Evans, X. Duan, Energy Environ. Sci. **9**, 2633 (2016)
54. C. Lei, M. Pi, P. Kuang, Y. Guo, F. Zhang, J. Coll. Interface Sci. **496**, 158 (2017)
55. R. Pourfaraj, S.J. Fatemi, S.Y. Kazemi, P. Biparva, J. Coll. Interface Sci. **508**, 65 (2017)
56. X. Wang, Y. Liu, H. Pang, S. Yu, Y. Ai, X. Ma, G. Song, T. Hayat, A. Alsaedi, X. Wang, Chem. Eng. J. **344**, 380 (2018)
57. R. Extremera, I. Pavlovic, M. Pérez, C. Barriga, Chem. Eng. J. **213**, 392 (2012)
58. O.P. Ferreira, O.L. Alves, D.X. Gouveia, A.G.S. Filho, J.A. de Paiva, J.M. Filho, J. Solid State Chem. **177**, 3058 (2004)
59. M. Shao, M. Wei, D.G. Evans, X. Duan, Chem. Eur. J. **19**, 4100 (2013)
60. C. Gao, X.-Y. Yu, T. Luo, Y. Jia, B. Sun, J.-H. Liu, X.-J. Huang, J. Mater. Chem. A **2**, 2119 (2014)
61. J. Xu, D. Xu, B. Zhu, B. Cheng, C. Jiang, Appl. Surf. Sci. **435**, 1136 (2018)
62. H.A. Prescott, Z.-J. Li, E. Kemnitz, A. Trunschke, J. Deutsch, H. Lieske, A. Auroux, J. Catal. **234**, 119 (2005)
63. R. Chimentao, S. Abelló, F. Medina, J. Llorca, J. Sueiras, Y. Cesteros, P. Salagre, J. Catal. **252**, 249 (2007)
64. H. Sontheimer, J.C. Crittenden, R.S. Summers, *Activated Carbon for Water Treatment* (DVGW-Forschungsstelle, Engler-Bunte-Institut, Universitat Karlsruhe, Karlsruhe, 1988)
65. R. Leggat, S. Taylor, S. Taylor, Coll. Surf. A Phys. Eng. Asp. **210**, 69 (2002)
66. E. Tombácz, M. Szekeres, Appl. Clay Sci. **34**, 105 (2006)
67. R. Leggat, S. Taylor, S. Taylor, Coll. Surf. A Phys. Eng. Asp. **210**, 83 (2002)
68. M.K. Nayunigari, R. Das, A. Maity, S. Agarwal, V.K. Gupta, J. Mol. Liq. **227**, 87 (2017)
69. S. Gamoudi, E. Srasra, J. Mol. Struct. **1193**, 522 (2019)
70. N.S.A. Mubarak, T. Chuan, H. Khor, A.H. Jawad, L. Wilson, S. Sabar, J. Polym, J. Polym. Environ. **29**, 1050 (2021)
71. S. Chilukoti, T. Thangavel, Inorg. Chem. Commun. **100**, 107 (2019)
72. R.-R. Shan, L.-G. Yan, Y.-M. Yang, K. Yang, S.-J. Yu, H.-Q. Yu, B.-C. Zhu, B. Du, J. Ind. Eng. Chem. **21**, 561 (2015)
73. D. Bharali, R.C. Deka, Coll. Sur.f A Phys. Eng. Asp. **525**, 64 (2017)
74. N. Hidayati, D. Apriliani, T. Taher, R. Mohadi, A. Lesbani, J. Phys. Conf. Ser. **1282**, 012075 (2019)
75. E. Fosso-Kankeu, F. Waanders, C.L. Fourie, Desalin. Water Treat. **57**, 27663 (2016)
76. R. Lafi, I. Montasser, A. Hafiane, Adsorpt. Sci. Technool. **37**, 160 (2019)
77. Y.-H. Jia, Z.-H. Liu, Coll. Surf. A Phys. Eng. Asp. **575**, 373 (2019)
78. J. Li, H. Yu, X. Zhang, R. Zhu, L. Yan, Front. Environ. Sci. Eng. **14**, 1 (2020)
79. H. Lyu, K. Hu, J. Fan, Y. Ling, Z. Xie, J. Li, Appl. Surf. Sci. **500**, 144037 (2020)
80. Q. Sun, M. Tang, P.V. Hendriksen, B. Chen, J. Alloy Compd. **829**, 154552 (2020)
81. B. Ali, B. Naceur, E. Abdelkader, E. Karima, B. Nourredine (2020) Int. J. Environ. Anal. Chem. **102**
82. Q. Sun, B. Chen, Ind. Eng. Chem. Res. **59**, 16838 (2020)

Authors and Affiliations

Hadja Alia Tabti[1] · Baghdad Medjahed[2] · Mohamed Boudinar[3] · Abdelkader Kadeche[1] · Noria Bouchikhi[1] · Amina Ramdani[4,5] · Safia Taleb[4] · Mehdi Adjdir[6,7]

[1]   Laboratory of Physico-Chemical Studies, University Dr. Moulay Tahar, 20000 Saida, Saida, Algeria

[2]   Laboratory of Separation and Purifcation Technology, Department of Chemistry, Faculty of Science, University of Tlemcen, Tlemcen, Algeria

[3]   Laboratory of Sciences, Technologies and Process Engineering, Department of Industrial Organic Chemistry, Faculty of Sciences, University of Sciences and Technology-Mohamed BOUDIAF of Oran (USTO-MB), Bir El Djir, BP 1505-EL M'naour, 31000 Oran, Algeria

[4]   Laboratory of Materials and Catalysis, Faculty of Sciences, Djillali Liabès's University, Site I BP 89, 22000 Sidi Bel-Abbès, Algeria

[5]   Department of Chemistry, Faculty of Sciences, University Dr. Moulay Tahar, 20000 Saida, Algeria

[6]   Laboratory of Applied Organic Synthesis, Faculty of Exact and Applied Sciences, University Oran1 Ahmed Ben Bella, BP 1524 El M'Naouer, 31000 Oran, Algeria

[7]   Department of Engineering Process, Faculty of Technology, University of Saida, Dr. Moulay Tahar, Saida, Algeria